JACS
JOURNAL OF THE AMERICAN CHEMICAL SOCIETY
COMMUNICATION
pubs.acs.org/JACS

Graphene Nanoribbons from Unzipped Carbon Nanotubes: Atomic Structures, Raman Spectroscopy, and Electrical Properties

Liming Xie,[†,§] Hailiang Wang,[†,§] Chuanhong Jin,[‡] Xinran Wang,[†] Liying Jiao,[†] Kazu Suenaga,[‡] and Hongjie Dai*[,†]

[†]Department of Chemistry, Stanford University, California 94305, United States

[‡]Nanotube Research Center, National Institute of Advanced Industrial Science and Technology (AIST), Tsukuba 305-8565, Japan

Supporting Information

ABSTRACT: We investigated the atomic structures, Raman spectroscopic and electrical transport properties of individual graphene nanoribbons (GNRs, widths ~10−30 nm) derived from sonochemical unzipping of multiwalled carbon nanotubes (MWNTs). Aberration-corrected transmission electron microscopy (TEM) revealed a high percentage of two-layer (2 L) GNRs and some single-layer ribbons. The layer−layer stacking angles ranged from 0° to 30° including average chiral angles near 30° (armchair orientation) or 0° (zigzag orientation). A large fraction of GNRs with bent and smooth edges was observed, while the rest showed flat and less smooth edges (roughness ≤1 nm). Polarized Raman spectroscopy probed individual GNRs to reveal D/G ratios and ratios of D band intensities at parallel and perpendicular laser excitation polarization ($D_{\parallel}/D_{\perp}$). The observed spectroscopic trends were used to infer the average chiral angles and edge smoothness of GNRs. Electrical transport and Raman measurements were carried out for individual ribbons to correlate spectroscopic and electrical properties of GNRs.

Graphene nanoribbons (GNRs) have been under intense investigation recently,[1−10] with various interesting chirality, width and edge-dependent electronic properties predicted.[11−13] Theoretically, tight-binding calculations have shown that two-thirds of armchair-edge GNRs are semiconducting and the other third and all zigzag-edge GNRs are metallic.[11] Ab initio calculations have shown that all GNRs exhibit band gaps, depending on chirality and ribbon width.[12] An interesting prediction has been reported that zigzag and chiral GNRs exhibit magnetic edge states[11,14] and half metallicity,[5] with potential applications in spintronics.

To probe interesting phenomena in GNRs, it is desirable to produce high-quality materials with well-defined structures in terms of chirality, width, and edge structures, and characterize by atomic-scale microscopy and spectroscopy to glean structure−property relations in GNRs. Bottom-up chemical approach[2] has produced atomically smooth GNRs with width of ~1 nm and length of ~30 nm. Lithography has fabricated GNRs with disordered edges.[7] And unzipping of carbon nanotubes (CNTs) have produced GNRs with various widths and lengths up to several micrometers.[3,4,6,15] In particular, GNRs derived in our lab by sonochemical unzipping of carbon nanotubes with minimum chemical oxidation have shown promising characteristics including smooth edges by scanning tunneling microscopy (STM),[14] the recently observed magnetic edge states in chiral GNRs,[14] and low resistivity[6] compared to ribbons derived by other methods.

Here, we present the first aberration-corrected transmission electron microscopy (TEM) investigation of GNRs (widths ~10−30 nm) derived from unzipping of multiwalled carbon nanotubes (MWNTs) to probe the atomic structures of GNRs including chiral angles, edge structures and smoothness. The results were correlated with polarized Raman spectroscopy measurements to understand the relations between the chirality and edge smoothness of GNRs and their polarized Raman signatures. Further, we have performed electrical transport and polarized Raman measurements of the same GNRs for understanding the electrical transport and Raman spectroscopic properties of GNRs.

GNRs, produced by sonochemical unzipping of MWNTs grown by arc-discharge in an organic polymer solution,[6] were deposited onto porous silicon membrane window grids for aberration-corrected TEM at an acceleration voltage of 80 or 60 kV. A large fraction of the GNRs showed Moiré patterns (Figure 1e,j and Figure 2b,g; coatings on the GNRs were polymer residues), indicating few-layer GNRs with non-AA/AB stacking inherited from the random stacking of concentric shells in the parent nanotubes.[16,17] The layer number of GNRs was estimated by the number of sets of hexagonal spots in the fast Fourier transform (FFT) of the TEM images (Figures 1f and 1k, Figures 2c, 2h and 2l). We found that two-layer (2 L) GNRs was dominant (~70%, Figure 2m) in our sample with ~6% of monolayer (1 L) GNRs (also observed by STM[14]) exhibiting a single set of hexagonal FFT spots (Figures 2k and 2l). The layer number was confirmed for several 2 L and 1 L GNRs by using a focused electron-beam to ablate and remove carbon atoms[18] from GNRs layer by layer (Figure S3 in Supporting Information [SI]). Also, due to the coexistence of nanotubes in the sample, we confirmed the flat nature (as opposed to cylindrical shape) of several ribbons by tilting the sample stage relative to the electron beam and observing reduced, projected widths of the ribbons (Figure S4 in SI).

The chiral angle of each layer in a GNR was determined by measuring the angle between the GNR axial direction and the zigzag direction (i.e., the $[1\bar{1}00]$ direction) of each layer from the FFT. We defined the zigzag direction to be at 0° chiral angle. Counter-clockwise direction from the zigzag line was defined to have positive chiral angles. While most of the GNRs showed random chiral angles for each layer (Figure.1d−h for a 2 L GNR

Received: April 27, 2011
Published: June 16, 2011

ACS Publications © 2011 American Chemical Society

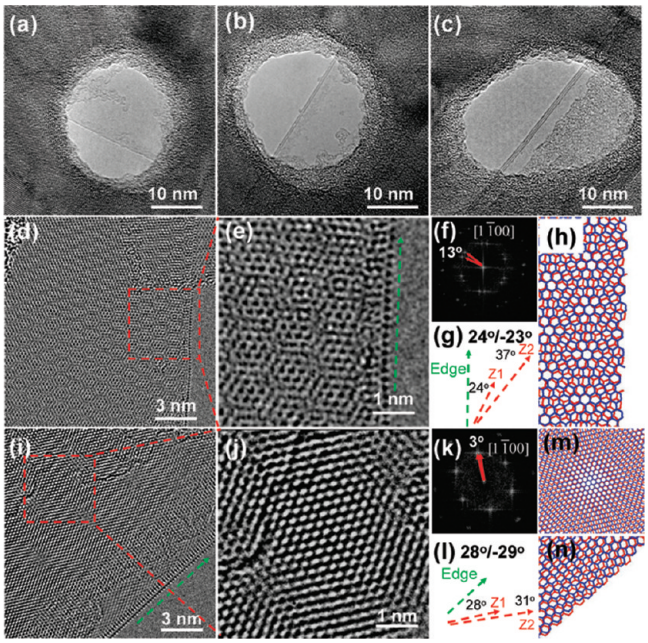

Figure 1. TEM images of GNRs with straight edge lines. (a−c) Low-magnification TEM images of GNRs with one, two, and three straight edge lines, respectively. Polymer residues are visible on the ribbons. (d) Large-scale TEM image, (e) zoomed-in TEM image, (f) FFT image, and (g) chiral angle analysis of a GNR with one straight edge line. (h) An atomic model of the GNR in panels (d) and (e). (i) Large-scale TEM image, (j) zoomed-in TEM image, (k) FFT image, and (l) chiral angle analysis of a GNR with two straight edge lines. (m,n) Atomic models of the GNR inside the GNR and near the edge respectively. The green dashed lines indicate GNR axial direction. The zigzag directions for each layer (Z1 and Z2, indicated by red dashed lines) for the different layers in panels (g) and (l) are derived from the [1$\bar{1}$00] directions (indicated by red arrows) in the corresponding FFT images.

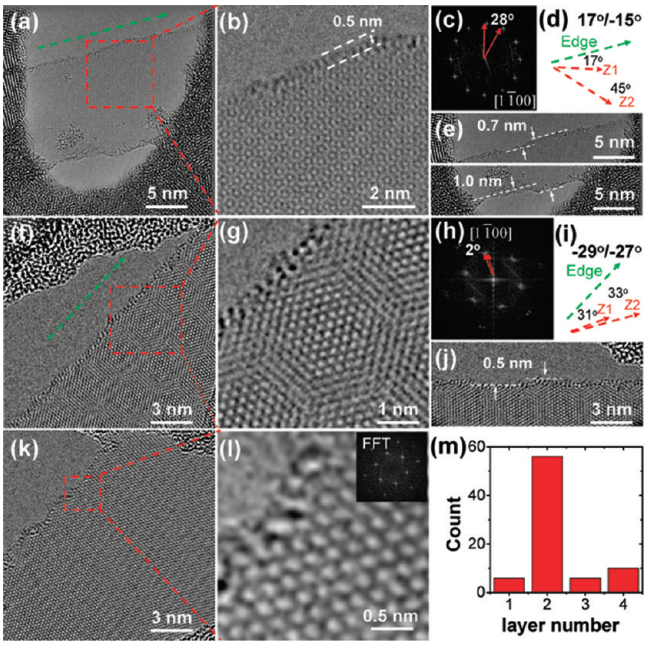

Figure 2. TEM images of GNRs with flat edges and distribution of GNR layer numbers. (a), (f) Large-scale TEM images, (b), (g) zoom-in TEM images, (c), (h) FFT images, (d), (i) chiral angle analysis, (e), (j) edge smoothness analysis of 2 L GNRs with flat edges. The green dashed lines indicate GNR axial directions. The zigzag directions (Z1 and Z2, indicated by red dash arrows) for the different layers in panel (d) and (i) are derived from the [1$\bar{1}$00] directions (indicated by red arrows) in the corresponding FFT images. (k) Large-scale TEM image, (l) zoomed-in TEM image of a 1 L GNR. (m) Distribution of layer numbers for GNRs in the sample.

with 24°/−23° chiral angles, and chiral angle distribution in Figure S5a in SI), we did observe a small fraction of 2 L GNRs with both layers oriented close to the armchair directions (Figure 1i−n for a GNR with 28°/−29° chiral angles) or close to the zigzag directions (Figure S6 in SI for a GNR with 0°/8° chiral angles). The layer−layer stacking for 2 L GNRs, measured from the rotation angle between the hexagonal spot sets in the FFT images, also ranged randomly from 0° to 30° (Figure S5b, SI).

TEM imaging revealed that many GNRs (66 out of 85) showed straight, parallel edge lines (Figures 1a−c). The dark, straight edge lines of the GNRs suggested likely bending at the edges, similar to bent edges observed in few-layer graphene sheets.[19] The edges of such ribbons appeared very smooth over relatively long ribbon lengths (straight edge lines in Figures 1a−c,d, and i), although the edge bending made it difficult to discern possible roughness out of the ribbon plane. We also observed GNRs with flat edges (19 out of 85) but without the dark parallel edge lines (Figures 2a,f,k). The edges of these ribbons tended to be less smooth with an edge roughness on the order of ∼1 nm (see Figure 2a,b,e for a GNR with edge roughness ∼1 nm over ∼20 nm length). A flat-edge GNR with relatively smoother edges is shown in Figure 2f,g,j (edge roughness <0.5 nm). For all of the GNRs imaged, we observed few obvious defects or disorders inside the GNR plane (Figures 1d,i, and 2a,f,k), indicating high quality of the GNRs.

In general, TEM revealed that the GNRs exhibited few defects in the plane, smooth edges (edge roughness ≤1 nm), random stacking between layers, and various chiral angles including GNRs with average layer orientations near armchair or zigzag directions. Next, we used polarized micro-Raman spectroscopy to characterize individual GNRs on SiO_2/Si substrates in the '*VV*' configuration (i.e., with the excitation laser polarization parallel to the polarization of the detected Raman signal; see Figure S2 in SI). For polarized Raman measurements, we used AFM imaging to select a relatively small percentage of GNRs with apparent topographic heights in the lowest range of 1.0−1.2 nm (including polymer residues on the ribbon) in the sample. These ribbons were likely 1 L GNRs although the possibility of 2 L could not be ruled out.

We observed four Raman bands for individual GNRs, including the disorder related D band at ∼1350 cm^{-1}, the graphitic G band at ∼1600 cm^{-1}, the D′ band at ∼1620 cm^{-1} (a disorder related intravalley double-resonance Raman band) and the 2D band at ∼2700 cm^{-1} (or G′ band, corresponding to an intervalley double-resonance Raman band) (Figure 3a−c). Since the layers in GNRs from unzipped MWNTs were generally non-AB stacked, we were unable to determine the layer number of our GNRs accurately based on the 2D profile. We found that the D and D′ bands of GNRs exhibited high polarization dependence, reaching maximum (or minimum) intensities when the laser-Raman polarization was parallel (or perpendicular) to the GNR direction (Figure 3a−c). On the other hand, the G and 2D bands showed weak polarization dependence for the 10−30 nm wide

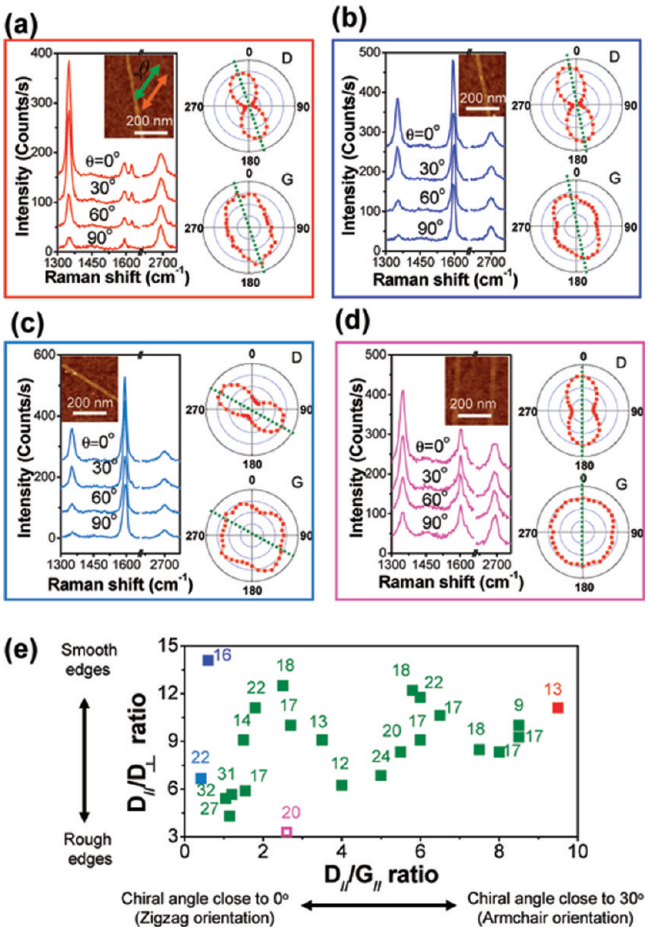

Figure 3. Polarized Raman spectra of GNRs (AFM height ~1.0−1.2 nm). (a) An individual GNR exhibiting a high $D_{\parallel}/G_{\parallel}$ ratio of 9.5 and a high $D_{\parallel}/D_{\perp}$ ratio of 11. (b) An individual GNR exhibiting a low $D_{\parallel}/G_{\parallel}$ ratio of 0.6 and a high $D_{\parallel}/D_{\perp}$ ratio of 14. (c) An individual GNR exhibiting a low $D_{\parallel}/G_{\parallel}$ ratio of 0.4 and a low $D_{\parallel}/D_{\perp}$ ratio of 6.7. (d) Data for lithographically patterned GNRs. The insets show AFM images for the corresponding GNRs. The intensity scales in all polar plots are linear starting from zero. The green dash lines indicate the GNR axial directions. Polarization dependence of D′ and 2D band intensities is shown in Figure S7 (SI). (e) $D_{\parallel}/D_{\perp}$ ratio vs $D_{\parallel}/G_{\parallel}$ ratio for all measured GNRs. The numbers near the data points are the corresponding GNR widths. The hollow square point represents the data for the Litho-GNRs in panel (d). The red, blue, and cyan points are the data for the GNRs in panels (a−c) with spectra in the corresponding colors.

GNRs, which differed from CNTs. The G band intensity approached zero at perpendicular laser polarization for individual SWNTs,[20] few-walled CNTs (Figure S8 in SI) and our GNR's parent MWNTs (Figure S9 in SI) measured in our control experiments.

With few defects in the plane of GNRs (TEM data in Figures 1 and 2), the observed D bands of the GNRs were likely due to the edges. Previous Raman spectroscopy of graphene edges showed high D/G ratios for near armchair edge orientations (chiral angles near 30°) due to favoring the intervalley resonance Raman processes responsible for the D band.[21−24] No D band or weak D band was expected for smooth zigzag edges due to the disfavored intervalley resonance for zigzag oriented edges. Therefore, we tentatively used the $D_{\parallel}/G_{\parallel}$ ratio (D band intensity over G band intensity at parallel polarization) to infer the chiral angle

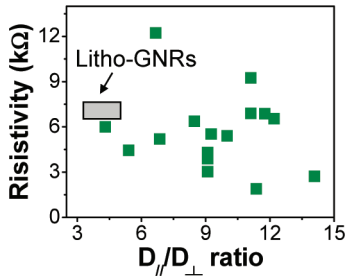

Figure 4. Plot of GNR resistivity vs $D_{\parallel}/D_{\perp}$ ratio for various GNRs (with AFM heights of 1.0−1.2 nm) used in polarized Raman measurements. Electrical transport measurements were done at room temperature. These ribbons were likely 1 L GNRs with an average resistivity higher than that of 1−3 nm tall GNRs (a high percentage of 2 L ribbons) measured previously (ref 6).

(or averaged chiral angles for possible 2 L GNRs selected for Raman experiments) of the ribbons. For more than 20 GNRs measured, the $D_{\parallel}/G_{\parallel}$ ratio spanned a large range from 0.4 to 9.5 (a near 25-fold variation, Figure 3e). GNRs with high $D_{\parallel}/G_{\parallel}$ ratio near 9.5 (Figure 3a) were assigned to GNRs with average chiral angles close to 30° (near armchair orientation) and GNRs with low $D_{\parallel}/G_{\parallel}$ ratios around 0.4 (Figure 3b and c) were assigned to GNRs with average chiral angles close to 0° (near zigzag orientation). GNRs with intermediate $D_{\parallel}/G_{\parallel}$ ratios (Figure S10 in SI) were assigned to chiral angles in between 0° and 30°.

The intensity ratio of the D band at parallel polarization ($D_{\parallel}$) and perpendicular polarization ($D_{\perp}$) measured at graphene edges have been suggested to reflect edge roughness and edge chirality.[21] A rougher edge generally exhibits lower $D_{\parallel}/D_{\perp}$ since the existence of disordered segments and random-orientated armchair segments can significantly increase $D_{\perp}$ intensity and hence lower the $D_{\parallel}/D_{\perp}$ ratio. The $D_{\parallel}/D_{\perp}$ ratios of near-zigzag (or near-armchair) edges are strongly (or weakly) dependent on edge roughness.[21] In our case, for GNRs with high $D_{\parallel}/G_{\parallel}$ ratios (~8−9.5, tentatively assigned to average chiral angle near 30° or near armchair orientation), high $D_{\parallel}/D_{\perp}$ ratios ($\gtrsim 8$) in a narrow range was typically observed (Figure 3e). For GNRs with low $D_{\parallel}/G_{\parallel}$ ratios (average chiral angle close to 0° or near zigzag orientation), the observed $D_{\parallel}/D_{\perp}$ ratios spanned a much wider range from ~14 down to ~4 (Figure 3e). These results were supportive of our assignment of GNRs with high (or low) $D_{\parallel}/G_{\parallel}$ ratios to ribbons with averaged orientations of the layers near the armchair (or zigzag) direction.

For comparison, we fabricated lithographically patterned GNRs (Litho-GNRs) with width of ~20 nm[25] (Figure 3d). The edges were known to be rough and disordered, causing transport gaps in Litho-GNRs observed experimentally.[7] Polarized Raman measurements of the Litho-GNRs found $D_{\parallel}/D_{\perp}$ ratios of ~3−4 (Figure 3d and the hollow square in e), obviously lower than $D_{\parallel}/D_{\perp}$ ratios of GNRs derived from nanotube unzipping. This spectroscopically confirmed that GNRs from unzipped MWNTs were of higher edge quality than Litho-GNRs.

We found that both $D_{\parallel}/G_{\parallel}$ and $D_{\parallel}/D_{\perp}$ ratios showed discernible increasing trends as the GNR width decreased in the 30 to 10 nm range (Figure S11 in SI), which is consistent with the measured electron coherence length of ~3 nm[26] near graphene edges and also the measured D/G ratio for Litho-GNRs by another group.[27] Different from few-layer graphene with non-AA/AB stacking,[28] the 2D/G intensity ratio cannot be used to indicate layer number for GNRs because the $2D_{\parallel}/G_{\parallel}$

ratio, as well as 2D width, was dependent on $D_{\parallel}/G_{\parallel}$ ratio (Figure S12 in SI). Theoretically, it was suggested that for GNRs[29,30] and graphene sheet edges the polarization dependence of G band intensity was different for zigzag and armchair edges.[31] However, the measured polarization dependence of the G band of our GNRs (Figure 3a−d) did not match with theoretical calculations,[29,30] which could be due to much wider ribbons measured here than in theoretical calculations. Further investigations are required to understand the differences.

We made electrical contacts to some of the individual GNRs with different $D_{\parallel}/G_{\parallel}$ and $D_{\parallel}/D_{\perp}$ ratios as measured by micro-Raman (Figure S13 in SI). Electrical transport measurements found no obvious dependence of GNR resistivity (defined as resistance at the Dirac point × GNR width/length) on $D_{\parallel}/G_{\parallel}$ ratio (Figure S13e). For various GNRs measured, a discernible trend of lower resistivity for GNRs with higher $D_{\parallel}/D_{\perp}$ ratios existed (Figure 4), consistent with reduced edge scattering in GNRs with smoother edges (higher $D_{\parallel}/D_{\perp}$).

In conclusion, atomic-scale TEM imaging was done for high-quality GNRs from unzipped MWNTs to reveal layer numbers, layer stacking, average chiral angles, and edge smoothness. The results were combined with polarized Raman to suggest that GNRs with $D_{\parallel}/G_{\parallel}$ ratio in the range of 0.4 to 9.5 corresponded to average chiral angles from 0° (zigzag oriented) to 30° (armchair oriented). GNRs with decreasing $D_{\parallel}/D_{\perp}$ ratio (in the range of 4−14) corresponded to a lower degree of edge smoothness (with lithography-derived GNRs exhibiting $D_{\parallel}/D_{\perp}$ ratio below 4), and the inferred edge roughness was consistent with electrical transport measurements of GNRs.

■ ASSOCIATED CONTENT

Supporting Information. Materials and methods and Figures S1−S13. This material is available free of charge via the Internet at http://pubs.acs.org.

■ AUTHOR INFORMATION

Corresponding Author
hdai1@stanford.edu

Author Contributions
[§]These authors contributed equally.

■ ACKNOWLEDGMENT

This work was supported by ONR, Graphene-MURI, MARCO-MSD, Intel and the NCEM at Lawrence Berkeley Lab, which was supported by the U.S. Department of Energy under Contract # DE-AC02-05CH11231. H.W. acknowledges Bin Jiang from FEI and Chengyu Song and Peter Ercius from NCEM for training and supervision on TEAM0.5 imaging. C.J. and K.S. acknowledge the support of JST-CREST.

■ REFERENCES

(1) Roche, S. *Nat. Nanotechnol.* **2011**, *6*, 8.
(2) Cai, J. M.; Ruffieux, P.; Jaafar, R.; Bieri, M.; Braun, T.; Blankenburg, S.; Muoth, M.; Seitsonen, A. P.; Saleh, M.; Feng, X. L.; Mullen, K.; Fasel, R. *Nature* **2010**, *466*, 470.
(3) Jiao, L. Y.; Zhang, L.; Wang, X. R.; Diankov, G.; Dai, H. J. *Nature* **2009**, *458*, 877.
(4) Kosynkin, D. V.; Higginbotham, A. L.; Sinitskii, A.; Lomeda, J. R.; Dimiev, A.; Price, B. K.; Tour, J. M. *Nature* **2009**, *458*, 872.
(5) Son, Y. W.; Cohen, M. L.; Louie, S. G. *Nature* **2006**, *444*, 347.
(6) Jiao, L. Y.; Wang, X. R.; Diankov, G.; Wang, H. L.; Dai, H. J. *Nat. Nanotechnol.* **2010**, *5*, 321.
(7) Han, M. Y.; Ozyilmaz, B.; Zhang, Y. B.; Kim, P. *Phys. Rev. Lett.* **2007**, *98*, 206805.
(8) Li, X. L.; Wang, X. R.; Zhang, L.; Lee, S. W.; Dai, H. J. *Science* **2008**, *319*, 1229.
(9) Cresti, A.; Nemec, N.; Biel, B.; Niebler, G.; Triozon, F.; Cuniberti, G.; Roche, S. *Nano Res.* **2008**, *1*, 361.
(10) Shimizu, T.; Haruyama, J.; Marcano, D. C.; Kosinkin, D. V.; Tour, J. M.; Hirose, K.; Suenaga, K. *Nat. Nanotechnol.* **2011**, *6*, 45.
(11) Nakada, K.; Fujita, M.; Dresselhaus, G.; Dresselhaus, M. S. *Phys. Rev. B* **1996**, *54*, 17954.
(12) Son, Y. W.; Cohen, M. L.; Louie, S. G. *Phys. Rev. Lett.* **2006**, *97*, 216803.
(13) Cresti, A.; Roche, S. *New J. Phys.* **2009**, *11*, 095004.
(14) Tao, C.; Jiao, L.; Yazyev, O. V.; Chen, Y.-C.; Feng, J.; Zhang, X.; Capaz, R. B.; Tour, J. M.; Zettl, A.; Louie, S. G.; Dai, H.; Crommie, M. F. *Nat. Phys.* **2011**10.1038/nphys1991.
(15) Jiao, L. Y.; Zhang, L.; Ding, L.; Liu, J. E.; Dai, H. J. *Nano Res.* **2010**, *3*, 387.
(16) Qin, L. C. *Phys. Chem. Chem. Phys.* **2007**, *9*, 31.
(17) Zuo, J. M.; Vartanyants, I.; Gao, M.; Zhang, R.; Nagahara, L. A. *Science* **2003**, *300*, 1419.
(18) Huang, J. Y.; Qi, L.; Li, J. *Nano Res.* **2010**, *3*, 43.
(19) Meyer, J. C.; Geim, A. K.; Katsnelson, M. I.; Novoselov, K. S.; Booth, T. J.; Roth, S. *Nature* **2007**, *446*, 60.
(20) Duesberg, G. S.; Loa, I.; Burghard, M.; Syassen, K.; Roth, S. *Phys. Rev. Lett.* **2000**, *85*, 5436.
(21) Casiraghi, C.; Hartschuh, A.; Qian, H.; Piscanec, S.; Georgi, C.; Fasoli, A.; Novoselov, K. S.; Basko, D. M.; Ferrari, A. C. *Nano Lett.* **2009**, *9*, 1433.
(22) Cancado, L. G.; Pimenta, M. A.; Neves, B. R. A.; Dantas, M. S. S.; Jorio, A. *Phys. Rev. Lett.* **2004**, *93*, 247401.
(23) Gupta, A. K.; Russin, T. J.; Gutierrez, H. R.; Eklund, P. C. *ACS Nano* **2009**, *3*, 45.
(24) You, Y. M.; Ni, Z. H.; Yu, T.; Shen, Z. X. *Appl. Phys. Lett.* **2008**, *93*, 163112.
(25) Wang, X. R.; Dai, H. J. *Nat. Chem.* **2010**, *2*, 661.
(26) Beams, R.; Cancado, L. G.; Novotny, L. *Nano Lett.* **2011**, *11*, 1177.
(27) Ryu, S.; Maultzsch, J.; Han, M. Y.; Kim, P.; Brus, L. E. *ACS Nano* **2011**, *5*, 4123.
(28) Reina, A.; Jia, X. T.; Ho, J.; Nezich, D.; Son, H. B.; Bulovic, V.; Dresselhaus, M. S.; Kong, J. *Nano Lett.* **2009**, *9*, 30.
(29) Sasaki, K.; Yamamoto, M.; Murakami, S.; Saito, R.; Dresselhaus, M. S.; Takai, K.; Mori, T.; Enoki, T.; Wakabayashi, K. *Phys. Rev. B* **2009**, *80*, 155450.
(30) Sasaki, K.; Saito, R.; Wakabayashi, K.; Enoki, T. *J. Phys. Soc. Jpn.* **2010**, *79*, 044603.
(31) Cong, C. X.; Yu, T.; Wang, H. M. *ACS Nano* **2010**, *4*, 3175.